VIMS Articles   Virginia Institute of Marine Science

2021

Sea-ice microbial communities in the Central Arctic Ocean: Limited responses to short-term pCO(2) perturbations

Anders Torstensson

Andrew R. Margolin
Virginia Institute of Marine Science

Gordon M. Showalter

Walker O. Smith Jr.
Virginia Institute of Marine Science

Elizabeth H. Shadwick
Virginia Institute of Marine Science

See next page for additional authors

Recommended Citation

Authors

Anders Torstensson, Andrew R. Margolin, Gordon M. Showalter, Walker O. Smith Jr., Elizabeth H. Shadwick, and et al

Sea-ice microbial communities in the Central Arctic Ocean: Limited responses to short-term pCO_2 perturbations

Anders Torstensson [icon],[1,2]* Andrew R. Margolin,[3,4] Gordon M. Showalter,[1] Walker O. Smith Jr,[3,5]
Elizabeth H. Shadwick,[3,6] Shelly D. Carpenter,[1] Francesco Bolinesi,[7] Jody W. Deming[1]
[1]School of Oceanography, University of Washington, Seattle, Washington
[2]Department of Ecology and Genetics, Limnology, Uppsala University, Uppsala, Sweden
[3]Virginia Institute of Marine Science, William & Mary, Gloucester Point, Virginia
[4]Institute for the Oceans and Fisheries, University of British Columbia, Vancouver, British Columbia, Canada
[5]School of Oceanography, Shanghai Jiao Tong University, Shanghai, China
[6]CSIRO Oceans and Atmosphere, Hobart, Tasmania, Australia
[7]Department of Biology, University of Napoli Federico II, Naples, Italy

Abstract

The Arctic Ocean is more susceptible to ocean acidification than other marine environments due to its weaker buffering capacity, while its cold surface water with relatively low salinity promotes atmospheric CO_2 uptake. We studied how sea-ice microbial communities in the central Arctic Ocean may be affected by changes in the carbonate system expected as a consequence of ocean acidification. In a series of four experiments during late summer 2018 aboard the icebreaker *Oden*, we addressed microbial growth, production of dissolved organic carbon (DOC) and extracellular polymeric substances (EPS), photosynthetic activity, and bacterial assemblage structure as sea-ice microbial communities were exposed to elevated partial pressures of CO_2 (pCO_2). We incubated intact, bottom ice-core sections and dislodged, under-ice algal aggregates (dominated by *Melosira arctica*) in separate experiments under approximately 400, 650, 1000, and 2000 μatm pCO_2 for 10 d under different nutrient regimes. The results indicate that the growth of sea-ice algae and bacteria was unaffected by these higher pCO_2 levels, and concentrations of DOC and EPS were unaffected by a shifted inorganic C/N balance, resulting from the CO_2 enrichment. These central Arctic sea-ice microbial communities thus appear to be largely insensitive to short-term pCO_2 perturbations. Given the natural, seasonally driven fluctuations in the carbonate system of sea ice, its resident microorganisms may be sufficiently tolerant of large variations in pCO_2 and thus less vulnerable than pelagic communities to the impacts of ocean acidification, increasing the ecological importance of sea-ice microorganisms even as the loss of Arctic sea ice continues.

Anthropogenic climate change is one of the largest threats to the marine environment, having negative effects on ecosystem functioning and habitat complexity (e.g., Hoegh-Guldberg and Bruno 2010). The ocean plays a crucial role to dampen the effects of global climate change. Since the beginning of the industrial period, the ocean has absorbed approximately 30%

of the anthropogenically emitted CO_2 and stores over 90% of all heat that has been trapped by increasing greenhouse gases (Sabine et al. 2004; IPCC 2013). Anthropogenic CO_2 inputs have already reduced average global sea surface pH by ~ 0.1, with models projecting a further decrease of 0.3–0.4 by the year 2100 (Caldeira and Wickett 2003; Orr et al. 2005; IPCC 2013). The Arctic Ocean is particularly vulnerable to rising atmospheric CO_2, as its relatively fresh water (mainly due to substantial riverine input) has a low buffering capacity, and the low water temperature promotes high CO_2 solubility. As a consequence, surface waters of the Arctic Ocean are projected to experience the largest pH decrease in the world in this century (ΔpH = -0.45), and be the first ocean to exhibit widespread undersaturation with respect to the carbonate mineral aragonite (Steinacher et al. 2009). Considering the importance of the Arctic Ocean for climate regulation (Vihma 2014) and the vibrancy of its ecosystems (Hoegh-Guldberg and Bruno 2010; Post et al. 2013), investigating the consequences of increased partial

Additional Supporting Information may be found in the online version of this article.

pressure of CO_2 (pCO_2) and reduced pH on marine organisms (i.e., ocean acidification) is essential.

The extensive sea-ice cover in polar seas provides a unique habitat for microbial assemblages. Sea ice is one of the largest biomes on the planet, covering 13% of Earth's surface at its maximum extent (Lizotte 2001). When sea ice forms and grows, internal channels containing highly saline water (brine) establish and create distinct habitats for microbial communities, which encompass members from multiple trophic levels such as small metazoans, unicellular algae, protozoa, bacteria, fungi, and viruses (Horner et al. 1992; Bowman et al. 2012; Torstensson et al. 2015a). Various algal assemblages generally dominate the biomass of these communities, particularly during spring and summer seasons, playing important roles in polar ecology and biogeochemistry (Arrigo and Thomas 2004; Arrigo 2017). In the central, ice-covered Arctic Ocean, sea-ice algae account for 57% of the primary production during summer (Gosselin et al. 1997) and are crucial food sources for many species of fish and invertebrates (Bluhm et al. 2017), especially during winter and early spring when the water column does not support significant phytoplankton production (Marschall 1988). These communities can be exposed to a wide range of pCO_2 as sea ice transitions from freeze up to melting. Sea-ice brine becomes oversaturated with gases, such as CO_2, during the formation of the ice as gases are concentrated in the brine. Convection of dense and CO_2-enriched brine creates a net downward transport of CO_2, referred to as the sea-ice pump (Rysgaard et al. 2011). In spring, primary production increases and the carbonate system in the brine equilibrates with the surrounding water and air, causing CO_2 undersaturation in the ice relative to the surrounding water. As a result, sea-ice microorganisms—especially brine communities in the interior sea ice—experience a much wider range of CO_2 concentrations compared to most planktonic species.

Sea-ice microorganisms also produce large amounts of extracellular polymeric substances (EPS), which are a broad group of compounds primarily composed of polysaccharides. EPS are abundant and key compounds in sea ice, having important roles in microbial acclimation in terms of cryoprotection, osmoprotection, motility, and adhesion (Deming and Young 2017). Microbially derived EPS can also alter sea-ice microstructure by clogging pores and acting to further depress the freezing point of the brine, which may enhance the habitability of sea ice (Krembs et al. 2011). These polymers are also known to be a major component of the cloud condensation nuclei in the high Arctic, and can therefore affect the chemistry and physics of Earth's atmosphere (Orellana et al. 2011). In framing this study, we hypothesized that the exudation of carbon-rich products, such as EPS and dissolved organic carbon (DOC), would increase as CO_2 levels rise and more inorganic carbon is consumed, leading to a shifted nutrient balance (increased inorganic C/N ratios), a process referred to as carbon overconsumption (Toggweiler 1993). Labile EPS also create an important link between the photoautotrophic and heterotrophic communities in sea ice (Deming and Young 2017), a link that may be altered if EPS production is enhanced. Overproduction of DOC has previously been described as a response to ocean acidification in a phytoplankton community in Kongsfjorden, Svalbard (Engel et al. 2013), but a similar scenario for sea-ice microbial communities is still unknown.

Although ocean acidification research on sea-ice microorganisms is a relatively new field, some coastal Antarctic studies have considered the effects of ocean acidification on sea-ice microorganisms and communities (e.g., McMinn et al. 2014; Cummings et al. 2019). The impacts of ocean acidification on Antarctic sea-ice microbial communities appear to be minimal, although a few studies suggest some species-specific physiological responses that can be either positive or negative responses (reviewed in McMinn 2017). However, similar studies on Arctic sea-ice microbial communities are absent, which is surprising given that ocean acidification is projected to have the largest impacts in the Arctic Ocean. An ability to scale and extrapolate between the poles is also limited, as the seasonality and vulnerability to ocean acidification differs between the Arctic and Antarctic (Shadwick et al. 2013), as does sea-ice thickness, snow cover, distribution, and biota (Arrigo 2017; Haas 2017). For instance, aggregates of the Arctic-endemic diatom *Melosira arctica* can reach lengths of several meters attached to the underside of Arctic sea ice using extensive EPS matrix material, playing an important role in carbon export in the central Arctic Ocean (Boetius et al. 2013). These communities are unique to the Arctic and host a diverse bacterial community, potentially indicating several important algal–bacterial interactions (Rapp et al. 2018). Still unknown, however, is how these communities may respond to future changes in the marine carbonate system.

As sea-ice microbial communities are exposed to a wide range of co-stressors along with ocean acidification—especially when the bottom ice community is dispersed into the water column following sea-ice melt—their response to ocean acidification and their ability to contribute to polar biogeochemical cycles will depend on their capacity to cope with changes in other environmental parameters, such as temperature, irradiance, salinity and nutrient distribution (Boyd and Hutchins 2012). For instance, a positive effect of elevated pCO_2 on carbon fixation rates could only be detected in a natural phytoplankton community in the Southern Ocean when the seawater was supplemented with iron (Hoppe et al. 2013). In addition, an increase in inorganic C/N ratio can cause imbalance between growth and photosynthesis in primary producers, leading to exudation of excess organic carbon that cannot be used for growth. Carbon overconsumption is therefore likely to be more noticeable under low nitrate conditions, suggesting that the combination of ocean acidification and inorganic nutrient depletion may stimulate microbial release of organic carbon. In this paper, we have studied how sea-ice microbial communities in the central Arctic Ocean are affected by changes in the carbonate system expected as a consequence

of ocean acidification under different nutrient regimes. In a series of four shipboard experiments, we addressed microbial growth, production of DOC and EPS, photosynthetic activity, and bacterial assemblage structure and diversity in sea ice at increasingly elevated CO_2 levels.

Methods

Experimental setup

Sea-ice cores and bottom aggregate communities were collected in the central Arctic Ocean at 88–90°N during August and September of the *Oden* Arctic Ocean 2018 expedition (Fig. 1; Table 1). For each experiment, we selected a sea-ice sampling plot of $\sim$ 10 m^2 and apparently homogeneous thickness. One full ice core was collected at each site, using a 0.09-m diameter Kovacs ice corer, for physicochemical characterization (temperature and bulk salinity) of the sea ice. Temperature in the core was recorded immediately after recovery, according to Torstensson et al. (2015a). The physicochemical core was then sectioned into 0.1-m sections, which were placed in gas-impermeable Tedlar® bags, and the atmosphere evacuated. After the ice sections melted at room temperature, bulk salinity was measured using a WTW Cond 3210™ conductivity meter. In addition, 40 experimental ice cores were taken within the selected plot, where 0.1-m bottom sections were removed from cores using a custom alloy bow-saw for ice sectioning. For each experimental unit, two randomly chosen bottom sections were placed in separate gas-tight Tedlar®

bags. Samples were returned to the ship where 2 L of filtered (0.2 μm) and chilled (-1.7°C) seawater were added to each bag, using either surface or deep water (10 or 1000 m, respectively; Table 1) to provide different nutrient concentrations. The samples were placed upright in water baths tempered to -1.7 ± 0.1°C, and irradiated with 15–18 μmol photons m^{-2} s^{-1} of constant photosynthetically active radiation (PAR) provided by fluorescent light tubes (Philips MASTER TL-D Super 80 36 W/865) and left to acclimate to the laboratory conditions until next day.

Four of the acclimated samples (four bags of two ice sections each) were thawed directly to serve as the initial time point. The morning after the acclimation period (Day 0), four treatments were initiated by injecting CO_2-saturated seawater (0.2 μm filtered, from either 10 or 1000 m, depending on the experiment; Table 1) into each of the remaining 16 bags to reach pCO$_2$ of approximately 400, 650, 1000, and 2000 μatm, with four replicates for each treatment (Fig. 2). These treatments approximately simulate the present-day pCO$_2$ (400 μatm), the atmospheric pCO$_2$ in 50 years derived using the present rate of increase (650 μatm), the estimate for the year 2100 (1000 μatm), and an extreme value that has already been observed in situ in Arctic sea ice during spring (2000 μatm; Geilfus et al. 2012). The amount of CO_2-saturated water needed to reach the different pCO$_2$ levels was calculated using the seacarb package in R (Gattuso et al. 2018; R Core Team 2018). The carbonate system and seawater salinity were monitored throughout the experiments by evacuating

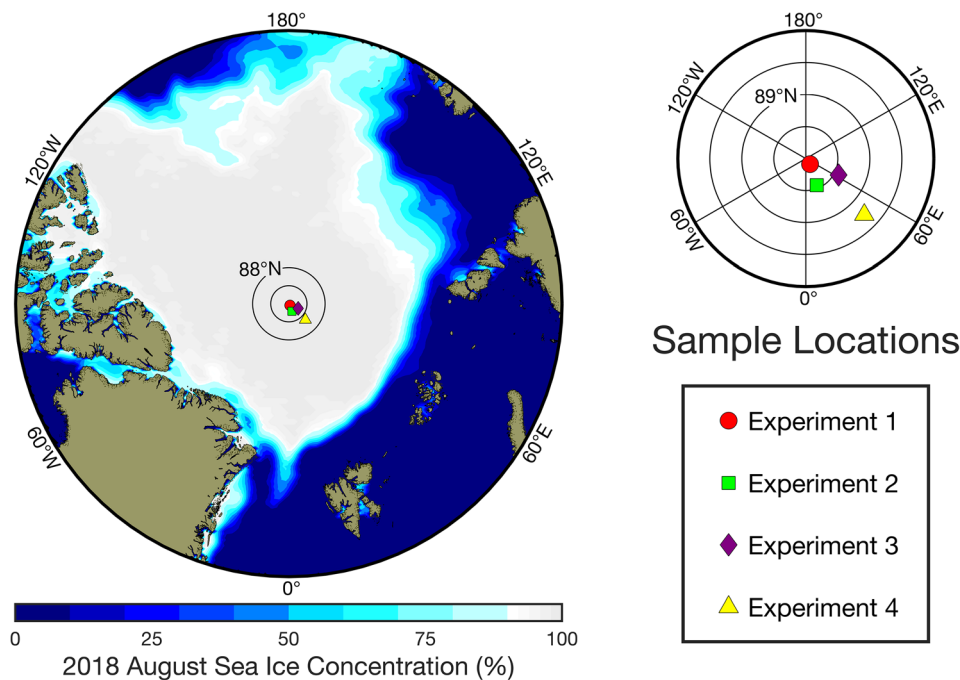**Fig. 1.** Arctic sea ice concentration (%) for August 2018, plotted to a southern latitude of 75°N with a gray mask for latitudes above $\sim$ 89°N. Sample locations are plotted for experiments 1 (red circle), 2 (green square), 3 (purple diamond) and 4 (yellow triangle). Sea ice concentration data are from the U.S. National Snow and Ice Data Center (Peng et al. 2013; Meier et al. 2017), plotted using M_Map (Pawlowicz 2019).

Table 1. Description of four ocean acidification experiments performed on sea-ice microbial communities during the *Oden* Arctic Ocean 2018 cruise.

Experiment	Community type	Collection date	Longitude (decimal degree)	Latitude (decimal degree)	Ice thickness (m)	Bottom ice temperature (°C)	Bottom ice bulk salinity	Collection depth of incubation water (m)	Salinity of incubation water
1	Core bottom	12 Aug 2018	37.2108	89.8902	1.52 (±0.05)	−1.41	2.8	1000	34.9
2	Core bottom	25 Aug 2018	22.2740	89.5508	1.38 (±0.01)	−1.64	3.1	1000	34.9
3	Aggregate	1 Sept 2018	63.4330	89.4273	(Not measured)	(Not measured)	(Not measured)	1000	34.9
4	Core bottom	7 Sept 2018	46.0600	88.7323	1.41 (±0.11)	−1.31	2.1	10	31.7

Sea-ice thickness from the ice-core experiments is presented as mean ± standard deviation ($n = 3$). Ice thickness where the dislodged algal aggregate was recovered from an ice hole was estimated at 1.5 m.

seawater subsamples from the bag's valve using a syringe and adjusting as needed (see Tables S1–S4 for specific time points). After 10 d of incubation, the samples were thawed at temperatures in the range of 4–10°C for 24–48 h, and subsampled directly after melting for the various biological parameters. For Experiment 3 (Table 1), a dislodged sea-ice aggregate community dominated by *M. arctica* was collected from a sampling hole in the ice and used instead of intact sea-ice sections. The aggregate was homogenized by gentle shaking and inoculated into Tedlar® bags containing seawater with the different targeted pCO_2 levels (400, 650, 1000, or 2000 μatm), and incubated and subsampled under the same conditions as described above. This experiment allowed for subsampling over time, and contained a more homogeneous starting community compared to the intact cores.

In summary, the four experiments (Table 1) were performed with either intact ice-core sections incubated in seawater with high initial nutrient concentrations (Experiments 1 and 2), *M. arctica* aggregates incubated in seawater with high initial nutrient concentrations (Experiment 3), or intact ice-core sections incubated in seawater with low initial nutrient concentrations (Experiment 4). These experiments allowed us to examine the effects of ocean acidification on different microbial communities, and under different inorganic nutrient conditions. A separate experiment was performed to verify that the carbonate system inside the ice sections had been perturbed, incubated under similar conditions as Experiments 1–4. In this experiment, the ice-core sections were removed from the seawater-filled bags after 6 d of incubation at the four pCO_2 levels, and thawed separately in atmosphere-evacuated Tedlar® bags for carbonate system determination.

Bulk community measurements

Samples for biological measurements were collected immediately after the ice cores had thawed completely, and all were processed at 4–10°C. Chlorophyll *a* (Chl *a*) concentration was measured using standard fluorometric techniques; subsamples of thawed materials were filtered through 25-cm Whatman GF/F filters, placed in 5 mL of 90% acetone (high-performance liquid chromatography grade), and extracted at 4°C for at least 24 h. Chl *a* was quantified on a Turner Designs Trilogy fluorometer using the nonacidification method (Welschmeyer 1994). The fluorometer was calibrated prior to the cruise using commercially purified Chl *a* (Sigma-Aldrich). Particulate organic carbon and nitrogen samples were collected by filtering known volumes through combusted (450°C for 2 h) Whatman GF/F filters (25 mm), rinsed with 5 mL of weak acid (0.01 N HCl in filtered seawater), stored in combusted glass vials covered with combusted aluminum foil, and dried at 60°C. Upon return to the laboratory, samples were combusted on a Costech 4100 elemental analyzer (Gardner et al. 2000). Particulate EPS (pEPS) samples were collected on 0.4-μm nucleopore filters and analyzed using the phenol–sulfuric acid assay (DuBois et al. 1956). Thawed subsamples were also fixed in 2% formaldehyde and stored at −20°C
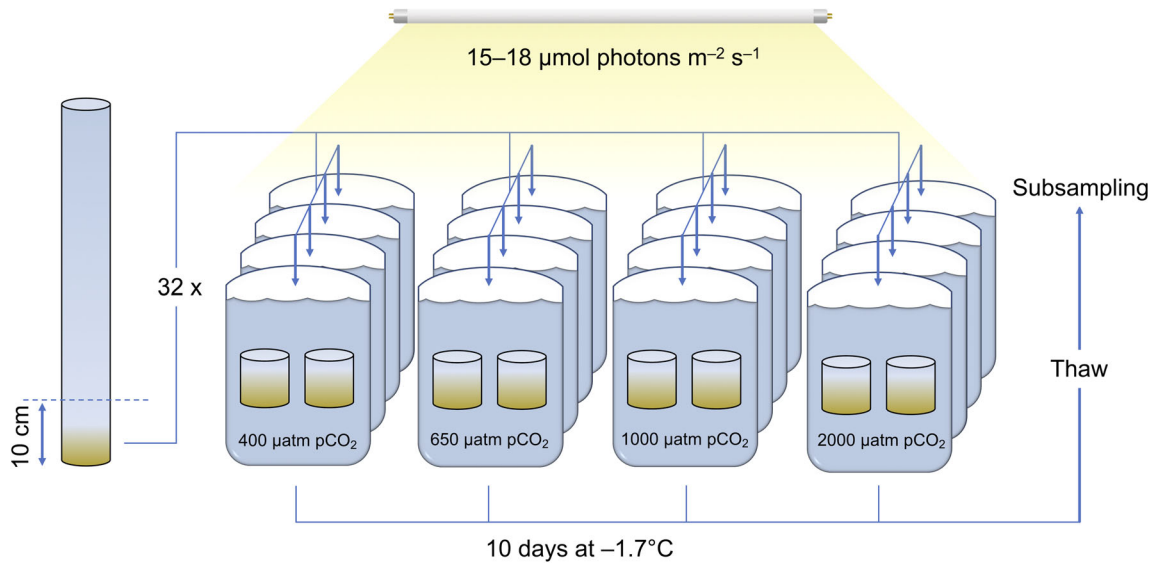
Fig. 2. Schematic view of the experimental setup. Bottom sections of sea-ice cores were collected from a 10-m^2 sampling plot of homogeneously thick sea ice, and incubated in filtered seawater in gas-tight bags with four different targeted pCO$_2$ levels (from 400 to 2000 μatm pCO$_2$) for 10 d under constant artificial light. Subsamples for seawater carbonate chemistry determination were evacuated from the bags 5–7 times during the experiments, and endpoint samples were thawed and subsampled for biological analyses at the end of the experiments. In Experiment 3, dislodged sea-ice algal aggregates were homogenized by shaking and distributed into bags as described above, instead of using intact ice-core sections.

until further processing and counting using epifluorescence microscopy and the stains 4′-6′-diamidino-2-phenylindole and N,N,N′,N′-tetramethylacridine-3,6-diamine (Acridine Orange). Filtrate (< 0.2 μm) from Experiments 1 and 3 was collected for analysis of DOC, frozen at −20°C, and analyzed using a Shimadzu TOC-Vcsh DOC analyzer; samples for inorganic nutrients were frozen at −20°C and analyzed using a QuAAtro autoanalyzer.

Variable fluorescence

Subsamples from Experiment 3 were taken for analyzing photosynthetic performance of the sea-ice algae by rapid light curves using pulse-amplitude modulated fluorometry (SubPAM; Gademann Instruments, Wuerzuburg, Germany). Cells were dark-adapted for a minimum of 60 min before measurements. The maximum (F_v/F_m) and effective quantum yields (Φ_{PSII}) of photosystem II (PSII) were measured. Minimum fluorescence (F_0) was determined by applying a low level of light and the maximum fluorescence (F_m) by exposing the sample to a short saturation pulse of measuring light (> 3000 μmol photons m^{-2} s^{-1} for 0.8 s). F'_m was determined for nondark-adapted cells. Variable fluorescence ($F_v = F_m − F_0$) and maximum quantum yield (F_v/F_m) were determined for all samples. Rapid light curves were performed by measurement of Φ_{PSII} $\left(\left[F'_m − F\right]/F'_m\right)$ of quasi-adapted (60 s) cells to stepwise increasing actinic light levels in the instrument's measuring unit (0, 25, 45, 66, 90, 125, 190, 285, and 420 μmol photons m^{-2} s^{-1}). The relative electron transport rate was then calculated as rETR = $\Phi_{PSII} \times$ PAR, where PAR is the photosynthetically active radiation in μmol photons m^{-2} s^{-1}. The saturating rapid light curves were fit using the exponential model from Platt

et al. (1980) so that the light saturation coefficient (E_k), the PSII efficiency (α_{PSII}), and the relative maximum ETR (rETR$_{max}$) could be calculated using the R package phytotools (Silsbe and Malkin 2015; R Core Team 2018).

Bacterial assemblage composition

Melted subsamples (455–1480 mL) from Experiments 1 and 3 were filtered through 0.2-μm Sterivex™ filter units or 0.2-μm polycarbonate filter discs, with the filters kept frozen at −80°C until processed. DNA was extracted from the filters using DNeasy PowerWater Kit (Qiagen, Sollentuna, Sweden), and DNA concentrations were quantified using PicoGreen (Invitrogen, Paisley, UK). The bacterial hypervariable regions V3/V4 of the 16S rRNA genes were amplified using the primer pair 341F (CCTACGGGNGGCWGCAG) and 805R (GACTACHVGGG TATCTAATCC), complemented with Illumina adapters. The amplicons were purified using MagSI beads (AMSBIO, Abingdon, UK) and amplified a second time using primers with sample-specific barcodes. After a second purification step and a subsequent DNA quantification using Quant-iT dsDNA HS assay (Invitrogen, Paisley, UK), the normalized DNA libraries were multiplexed and sequenced by Illumina MiSeq technology using a 2 × 300 bp configuration (National Genomics Infrastructure, SciLifeLab, Stockholm, Sweden).

Quality filtering, denoising, and removal of potential chimeras and nonbacterial DNA sequences from the demultiplexed sequences were performed using the nf-core/amplicon 1.1.2 pipeline (Straub et al. 2019). In short, raw data were quality-controlled using FastQC v.011.8 (Andrews 2010), primers were trimmed using Cutadapt v.2.6 (Martin 2011), data were

imported into QIIME2 v2019.10.0 (Bolyen et al. 2019) where potential chimeras were removed and amplicon sequencing variants (ASVs) were generated using DADA2 (Callahan et al. 2017) and classified against the SILVA v.132 database (Quast et al. 2013). All chloroplast and mitochondria sequences were removed in DADA2 to enable comparisons between samples. Archaeal reads (seven reads in total) were removed from the ASV table, and further statistical analyses were performed in the R package phyloseq v.1.32.0, including determination of alpha diversity (Chao1 and Shannon's indices) (McMurdie and Holmes 2013; R Core Team 2018). All sequences obtained in this study have been deposited in the Sequence Read Archive under BioProject ID PRJNA647311.

Carbonate system

Dissolved inorganic carbon (DIC) concentrations were measured using an Automated Infra-Red Inorganic Carbon Analyzer (AIRICA) coupled with a LI-COR LI-7000 CO_2/H_2O Analyzer, having a manufacturer precision typical of 1.5 μmol kg^{-1} (http://www.marianda.com). To initiate the AIRICA, "junk" seawater was analyzed until a coefficient of variance (CV) less than 2 μmol kg^{-1} was obtained. To calibrate the AIRICA, a certified reference material (CRM, provided by Andrew G. Dickson, Scripps Institute of Oceanography, CA) was analyzed to establish a "conversion factor" that was applied so the following CRMs were within 2 μmol kg^{-1} of the certified concentration. A CRM was analyzed every eight samples and before the AIRICA was turned off to correct for instrument drift, and CRMs and samples were rerun if the CV was greater than 2 μmol kg^{-1}. For typical junk, CRM and sample analyses, a total of 10 mL of seawater was drawn to flush the instrument and analyze 1 mL in triplicate.

Analysis of DIC was always conducted first, followed by pH and salinity. Syringes were connected directly to the AIRICA's intake valve so any exposure to the atmosphere was avoided. Once an acceptable value was obtained from the AIRICA, the syringe was opened so that pH could be analyzed promptly.

Seawater voltage and analysis temperature were measured using a Mettler Toledo SG78 pH electrode, which was calibrated by a 2-amino-2-hydroxymethyl-1,3-propanediol (TRIS) buffer (provided by Andrew G. Dickson, Scripps Institute of Oceanography, CA) for converting measured voltages to pH on the total scale (pH$_T$) (DelValls and Dickson 1998). TRIS buffer was measured at the beginning of every set of samples. To asses electrode drift, we began measuring TRIS buffer after finishing sample analysis and/or between experimental analyses on August 29, increasing this frequency to every 4–5 samples for the final 2 d of analysis on September 16 and 18. Salinity was measured using a WTW Cond 3210™ conductivity meter.

Following measurement of DIC and pH$_T$, total alkalinity (TA) and pCO$_2$ were computed using the CO2sys program of van Heuven et al. (2011), and the carbonic acid dissociation constants of Roy et al. (1993). Several high-latitude Arctic studies have addressed the differences in derived carbonate

parameters associated with the choice of the carbonic acid constant in both sea ice (e.g., Chierici and Fransson 2009; Fransson et al. 2013) and seawater (Woosley et al. 2017) by internal consistency checks between the four carbonate system parameters (i.e., DIC, TA, pH, and pCO$_2$). Following the determination of Chierici and Fransson (2009) for suitability for Arctic sea ice, we used the Roy et al. (1993) constants. In the absence of phosphate and silicate measurements, we used null values for these two nutrients in the carbonate system computations. While this approach introduces additional uncertainty to the computed parameters, the added uncertainty is smaller than the standard deviation of the computed parameters, which here is used as an overall estimate of uncertainty.

Statistical analysis

All univariate data were analyzed using one-way ANOVA or two-way repeated measures ANOVA. Levene's test was used to test for heteroskedasticity; if the assumptions for ANOVA were not met, data were log-transformed. Possible significant effects were explored using Tukey's honestly significant difference (HSD) test. Nonmetric multidimensional scaling of the bacterial composition was performed using Bray–Curtis dissimilarity, using the phyloseq package in R (McMurdie and Holmes 2013; R Core Team 2018). Hypotheses about differences in the structure of bacterial assemblages between pCO$_2$ treatments were evaluated using permutational ANOVA (PERMANOVA) with subsequent pairwise comparisons, using 999 permutations in the vegan package in R (R Core Team 2018; Oksanen et al. 2019). Differential abundance analysis was performed to identify specific ASVs affected by the experimental treatments, using analysis of composition of microbiomes (ANCOM) in R (Mandal et al. 2015). The ANCOM procedure compares the relative abundance of a taxon between groups by calculating Aitchison's log-ratio of abundance (Aitchison 1982) of each taxon relative to the abundance of all remaining taxa one at a time, resulting in a test constrained to reduce false discovery rates while maintaining high statistical power. ASVs representing 90% of the total abundance and with a total read count > 1000 were included in the ANCOM. A probability level (p) of < 0.05 was used for statistical significance in all tests.

Log-response ratios (lnRR) were calculated for every sample and was used to visualize the responses relative to the mean of the control treatment (i.e., the 400 μatm treatment). They were calculated as:

$$\ln RR = \ln\left(X \div \bar{X}_C\right), \tag{1}$$

where lnRR is the natural-log proportional change between a sample value (X) and the mean of the 400 μatm treatment ($\bar{X}_C$).

Results

Environmental and experimental conditions

The physicochemical ice cores had bottom-ice temperatures that ranged from $-1.64°C$ to $-1.31°C$, and had bulk salinities

Table 2. Carbonate system parameters (mean $\pm$ standard deviation) in the seawater surrounding sea-ice microbial communities over 5–7 time points (four replicates each) during four ocean acidification experiments.

Experiment	Targeted pCO$_2$ treatment (μatm)	Achieved pCO$_2$ (μatm)	pH$_T$	DIC (μmol kg^{-1})	Salinity	n
1	400	349 $\pm$ 76	8.051 $\pm$ 0.090	1987 $\pm$ 67	32.7 $\pm$ 1.8	28
	650	705 $\pm$ 183	7.773 $\pm$ 0.102	2072 $\pm$ 83	32.9 $\pm$ 2.0	27
	1000	945 $\pm$ 135	7.639 $\pm$ 0.056	2092 $\pm$ 79	32.7 $\pm$ 1.8	28
	2000	1767 $\pm$ 328	7.382 $\pm$ 0.089	2179 $\pm$ 77	32.6 $\pm$ 2.0	27
2	400	263 $\pm$ 58	8.163 $\pm$ 0.079	1936 $\pm$ 82	30.9 $\pm$ 1.0	19
	650	549 $\pm$ 129	7.888 $\pm$ 0.107	2055 $\pm$ 85	31.1 $\pm$ 1.4	19
	1000	767 $\pm$ 136	7.736 $\pm$ 0.068	2097 $\pm$ 88	31.2 $\pm$ 1.0	19
	2000	1552 $\pm$ 243	7.434 $\pm$ 0.066	2180 $\pm$ 74	30.9 $\pm$ 1.0	16
3	400	362 $\pm$ 79	8.070 $\pm$ 0.088	2169 $\pm$ 21	34.6 $\pm$ 0.1	20
	650	789 $\pm$ 185	7.759 $\pm$ 0.101	2271 $\pm$ 23	34.6 $\pm$ 0.2	20
	1000	1128 $\pm$ 272	7.612 $\pm$ 0.104	2318 $\pm$ 27	34.6 $\pm$ 0.2	20
	2000	1784 $\pm$ 388	7.419 $\pm$ 0.094	2393 $\pm$ 24	34.6 $\pm$ 0.2	20
4	400	300 $\pm$ 48	8.124 $\pm$ 0.066	2036 $\pm$ 32	31.2 $\pm$ 0.5	20
	650	524 $\pm$ 75	7.899 $\pm$ 0.055	2093 $\pm$ 45	30.9 $\pm$ 0.6	20
	1000	795 $\pm$ 147	7.732 $\pm$ 0.074	2154 $\pm$ 36	31.2 $\pm$ 0.6	20
	2000	1542 $\pm$ 204	7.451 $\pm$ 0.057	2225 $\pm$ 43	30.7 $\pm$ 0.6	20

The carbonate system was readjusted to the targeted treatment level after measurement at specific time points (see Tables S1–S4). Achieved pCO$_2$ was calculated using pH$_T$ and DIC.

Table 3. Mean values $\pm$ standard deviation (n = 4) for chlorophyll a (Chl a) concentration, bacterial abundance (bacteria), dissolved organic carbon (DOC) and particulate extracellular polymeric substances (pEPS) concentration, particulate organic carbon to nitrogen ratio (C/N), and inorganic nutrient concentrations in four experiments with sea-ice microbial communities before starting incubation (initial) and after 10 d under four pCO$_2$ treatments (400, 650, 1000, and 2000 μatm).

| Exp	Targeted pCO$_2$ treatment (μatm)	Chl a (μg L^{-1})	Bacteria (10^6 cells mL^{-1})	DOC (mg L^{-1})	pEPS (μg glu EQ mL^{-1})	C/N (w/w)	NO$_2$ + NO$_3$ (μM)	Si (μM)	PO$_4$ (μM)
1	Initial	14.1 $\pm$ 2.0	0.75 $\pm$ 0.16	0.73 $\pm$ 0.13	0.32 $\pm$ 0.05	12.7 $\pm$ 1.8	28.7 $\pm$ 6.1	13.5 $\pm$ 3.8	1.46 $\pm$ 0.26
	400	16.0 $\pm$ 4.3	1.03 $\pm$ 0.36	0.46 $\pm$ 0.11	0.18 $\pm$ 0.06	8.8 $\pm$ 1.3	16.8 $\pm$ 4.2	6.7 $\pm$ 1.3	0.67 $\pm$ 0.16
	650	22.4 $\pm$ 5.0	1.28 $\pm$ 0.53	0.73 $\pm$ 0.20	0.28 $\pm$ 0.02	9.8 $\pm$ 1.1	19.6 $\pm$ 2.1	7.6 $\pm$ 0.9	0.90 $\pm$ 0.07
	1000	18.9 $\pm$ 3.6	1.20 $\pm$ 0.19	0.58 $\pm$ 0.04	0.24 $\pm$ 0.07	9.5 $\pm$ 1.3	16.1 $\pm$ 5.0	6.8 $\pm$ 1.0	0.76 $\pm$ 0.19
	2000	17.7 $\pm$ 2.9	1.22 $\pm$ 0.22	0.51 $\pm$ 0.14	0.24 $\pm$ 0.06	11.1 $\pm$ 0.4	13.0 $\pm$ 2.3	5.8 $\pm$ 1.1	0.61 $\pm$ 0.09
2	Initial	5.2 $\pm$ 1.3	0.61 $\pm$ 0.19	No data	0.15 $\pm$ 0.10	19.6 $\pm$ 3.0	23.1 $\pm$ 0.6	8.31 $\pm$ 0.6	1.19 $\pm$ 0.04
	400	22.4 $\pm$ 2.9	0.80 $\pm$ 0.12	No data	0.40 $\pm$ 0.12	11.8 $\pm$ 1.1	1.3 $\pm$ 2.2	0.80 $\pm$ 0.2	0.14 $\pm$ 0.05
	650	21.4 $\pm$ 4.0	0.77 $\pm$ 0.19	No data	0.38 $\pm$ 0.06	12.2 $\pm$ 1.5	0.3 $\pm$ 0.1	0.93 $\pm$ 0.3	0.17 $\pm$ 0.02
	1000	22.4 $\pm$ 7.5	0.89 $\pm$ 0.11	No data	0.58 $\pm$ 0.16	12.8 $\pm$ 1.9	0.2 $\pm$ 0.1	0.80 $\pm$ 0.3	0.14 $\pm$ 0.04
	2000	16.2 $\pm$ 3.8	0.67 $\pm$ 0.45	No data	0.46 $\pm$ 0.17	13.0 $\pm$ 0.7	0.5 $\pm$ 0.5	1.37 $\pm$ 0.8	0.25 $\pm$ 0.09
3	Initial	4.4 $\pm$ 0.6	0.12 $\pm$ 0.01	1.49 $\pm$ 0.25	0.16 $\pm$ 0.03	17.1 $\pm$ 1.3	28.5 $\pm$ 1.1	8.21 $\pm$ 0.3	1.56 $\pm$ 0.07
	400	25.3 $\pm$ 0.7	0.85 $\pm$ 0.08	1.53 $\pm$ 0.25	0.26 $\pm$ 0.04	7.6 $\pm$ 0.8	0.2 $\pm$ 0.1	0.52 $\pm$ 0.2	0.03 $\pm$ 0.01
	650	23.8 $\pm$ 2.5	0.80 $\pm$ 0.07	1.66 $\pm$ 0.21	0.19 $\pm$ 0.02	8.1 $\pm$ 1.6	0.1 $\pm$ 0.02	0.54 $\pm$ 0.3	0.10 $\pm$ 0.09
	1.000	25.9 $\pm$ 1.1	0.76 $\pm$ 0.08	1.45 $\pm$ 0.25	0.27 $\pm$ 0.01	8.1 $\pm$ 0.9	0.2 $\pm$ 0.03	0.52 $\pm$ 0.2	< 0.02
	2.000	24.9 $\pm$ 1.6	0.74 $\pm$ 0.08	1.37 $\pm$ 0.30	0.21 $\pm$ 0.03	7.3 $\pm$ 0.3	0.2 $\pm$ 0.09	0.55 $\pm$ 0.1	< 0.02
4	Initial	8.9 $\pm$ 1.6	0.75 $\pm$ 0.09	No data	0.28 $\pm$ 0.09	12.2 $\pm$ 1.6	1.1 $\pm$ 0.4	7.3 $\pm$ 3.2	0.57 $\pm$ 0.06
	400	6.8 $\pm$ 2.6	0.94 $\pm$ 0.24	No data	0.51 $\pm$ 0.11	19.0 $\pm$ 1.1	1.6 $\pm$ 0.5	2.8 $\pm$ 1.0	0.25 $\pm$ 0.07
	650	7.7 $\pm$ 1.6	0.80 $\pm$ 0.01	No data	0.53 $\pm$ 0.08	19.0 $\pm$ 0.1	2.2 $\pm$ 1.2	2.8 $\pm$ 1.0	0.23 $\pm$ 0.05
	1.000	6.8 $\pm$ 2.1	0.91 $\pm$ 0.08	No data	0.45 $\pm$ 0.19	18.6 $\pm$ 0.9	1.9 $\pm$ 0.5	3.3 $\pm$ 0.8	0.24 $\pm$ 0.02
	2.000	7.6 $\pm$ 0.8	1.02 $\pm$ 0.19	No data	0.54 $\pm$ 0.17	16.8 $\pm$ 2.1	1.3 $\pm$ 0.5	3.9 $\pm$ 0.5	0.36 $\pm$ 0.07
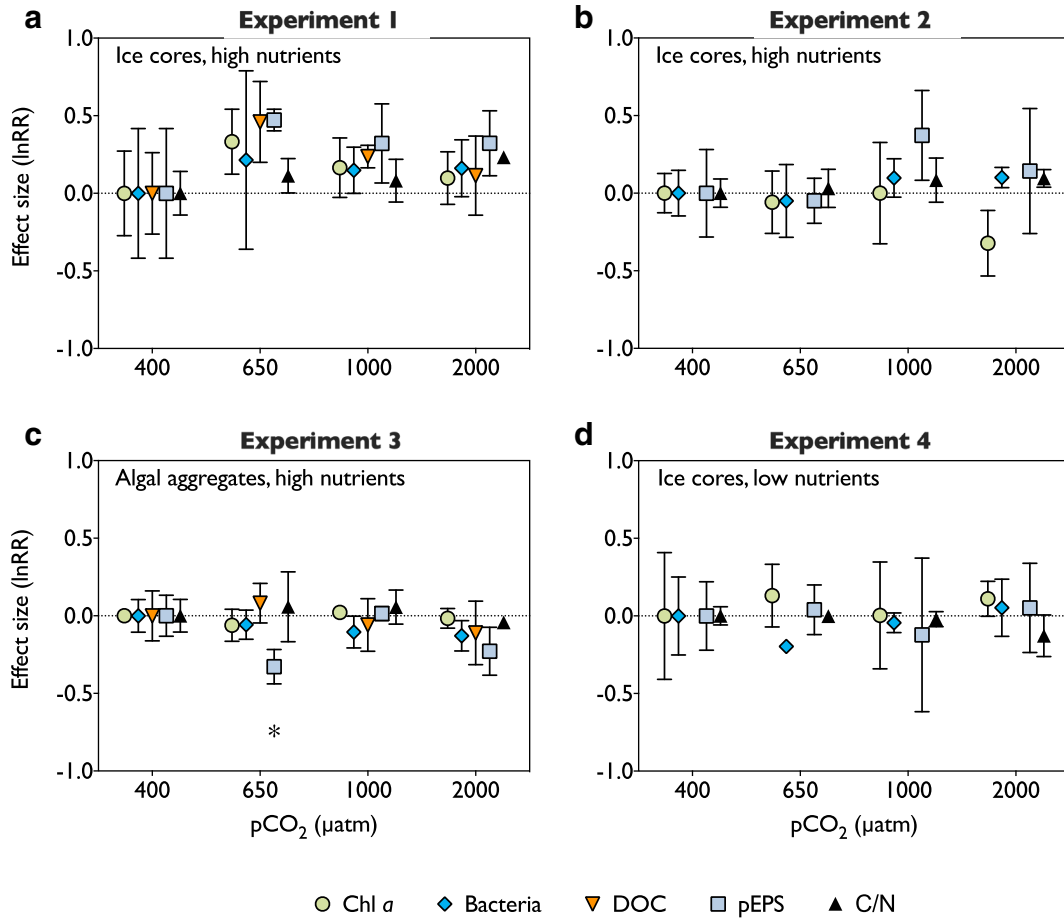
Fig. 3. Effect sizes of concentrations of chlorophyll *a* (Chl *a*), bacterial abundance (bacteria), dissolved organic carbon (DOC), particulate extracellular polymeric substances (pEPS), and particulate organic carbon to nitrogen ratios (C/N) are expressed as log response ratios (lnRR) relative to the control treatment (400 μatm pCO_2) for each experiment. As a result, the mean lnRRs of the 400 μatm pCO_2 treatment always equals zero. The only statistically significant finding (noted with asterisk) was in Experiment 3 (algal aggregates), where the mean pEPS concentration in the 650 μatm pCO_2 treatment was lower than the mean value the control treatment (400 μatm pCO_2). Error bars show standard deviation ($n = 4$); where not visible, bars were smaller than the symbol.

between 2.1 and 3.1 (Table 1). During the experiments, the pCO_2 in the seawater differed significantly between all treatments in the respective experiment when averaged over all time points ($p < 0.0001$, repeated measure ANOVAs; Table 2). The pCO_2 also differed significantly for each specific time point ($p < 0.05$, Tukey's HSD; Tables S1–S4), except between the 650 and 1000 μatm treatments at Day 0 in Experiment 1 ($p = 0.746$, Tukey's HSD) and between the 400 and 650 μatm treatments at Day 6 in Experiment 4 ($p = 0.112$, Tukey's HSD). However, the pCO_2 was typically below targeted values at the time of sampling (Table 2). The average seawater salinity decreased in the experiments containing sea-ice sections, from 34.9 to 29.6 in Experiment 1, 32.8 to 29.8 in Experiment 2, and 31.2 to 30.4 in Experiment 4; it remained unchanged throughout the (ice-free) algal aggregate Experiment 3 (Tables S1–S4). The inorganic nutrient concentrations were generally high in the beginning of Experiments 1–3 (sea-ice microbial communities incubated with deep water), then decreased modestly during

Experiment 1 and substantially during Experiments 2 and 3 (Table 3). In Experiment 4 (ice cores incubated with surface water), the inorganic nutrient concentrations remained low throughout the experiment (Table 3).

The mean ($\pm$ standard deviation) temperature in the water baths was -1.7 (± 0.1)$°$C throughout all experiments. Less melting was apparent in Experiment 4, where the temperature was closer to the freezing point of the less saline surface seawater (10 m), compared to the deep water (1000 m) in Experiments 1–3. The ice-core sections in Experiments 1, 2, and 4 appeared intact with visual filaments of sea-ice algae at the end of the incubations.

Bulk community responses

The growth of algae (as determined by changes in concentration of Chl *a*) and bacteria (as epifluorescent counts) was observed in Experiments 1–3, but not in Experiment 4, where the ice-core sections had been incubated with
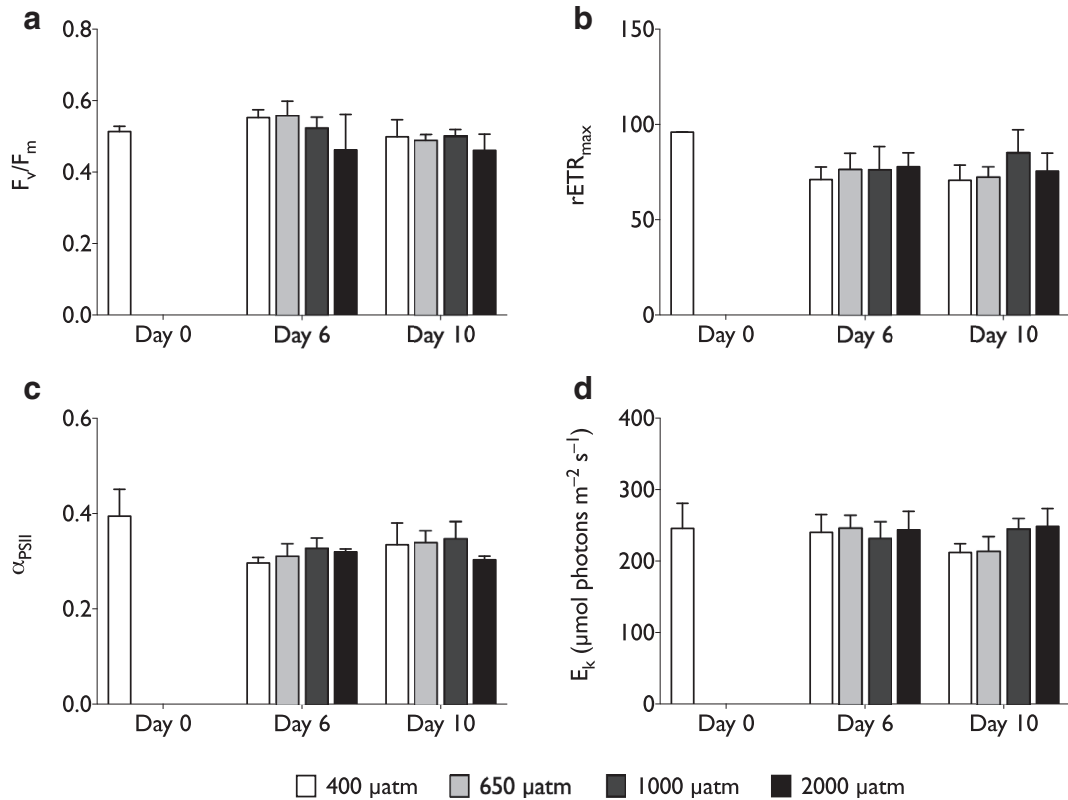
Fig. 4. Time-course evaluation of photosynthetic parameters under four pCO_2 treatments (targeting 400, 650, 1000, and 2000 μatm) during Experiment 3. No significant affect was observed for any of the photosynthetic parameters measured: (**a**) maximum quantum yield (F_v/F_m), (**b**) maximum relative electron transport rate (rETR$_{max}$), (**c**) photosystem II efficiency (α_{PSII}), and (**d**) the light saturation coefficient (E_k). The data were obtained from rapid light curves using pulse-amplitude modulated-fluorometry. Error bars represent standard deviation ($n = 4$).
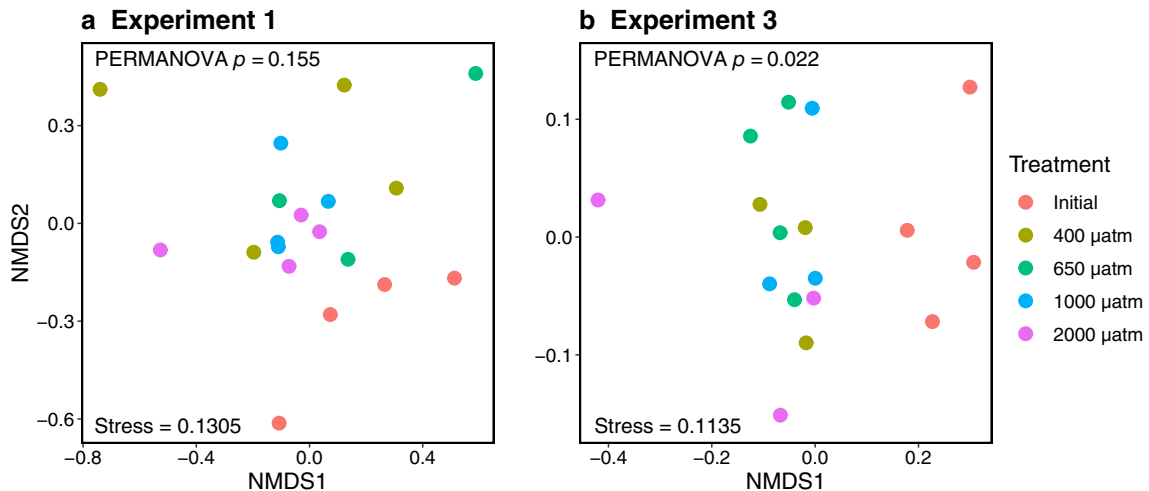
Fig. 5. Nonmetric multidimensional scaling of bacterial assemblage composition in Experiments 1 (**a**) and 3 (**b**), based on Bray–Curtis dissimilarity of ASV abundance. The color of each sample represents pCO_2 treatment.

nutrient-poor surface water (Table 3). In Experiment 1, Chl *a* concentrations increased moderately in all treatments from 14.1 to 18.7 μg L^{-1}, whereas in Experiments 2 and 3, they increased substantially from 5.2 to 20.6 and 4.4 to

25.0 μg L^{-1}, respectively. During Experiment 4, the Chl *a* concentrations decreased from 8.9 to 7.2 μg L^{-1}. Here, organic C/N ratios increased during the experiment, whereas these ratios decreased in Experiments 1–3 (Table 3).
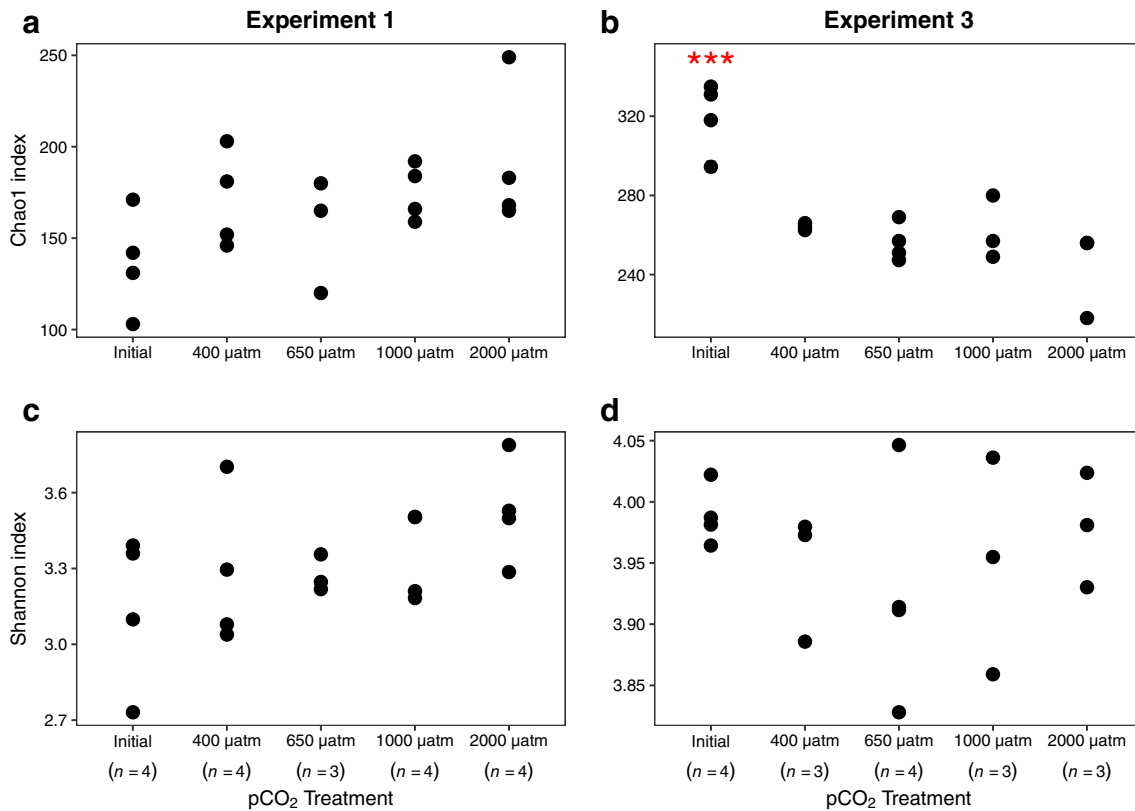
Fig. 6. Bacterial community richness (**a**,**b**) and diversity (**c**,**d**) in experiments 1 and 3. Asterisks denote statistical significance ($p < 0.001$), where the Chao1 index was higher in the initial samples than in any of the treatments after 10 d of incubation.

Bacterial abundances followed similar patterns as Chl a concentrations, except for Experiment 2, where Chl a concentrations increased substantially but bacterial abundances only increased modestly (Table 3). Concentrations of pEPS decreased during Experiment 1 and increased in Experiments 2–4 (Table 3).

Increased pCO_2 did not have any significant effects on Chl a concentrations, bacterial abundances, DOC concentrations or C/N ratios in any of the experiments ($p > 0.05$, ANOVA, Fig. 3; Table 3). Concentration of pEPS was significantly affected by the treatments in Experiment 3 ($p = 0.006$, $F_{3,11} = 7.3$, ANOVA; Fig. 3c; Table 3), where the 650 μatm treatment had lower concentrations than the control ($p = 0.021$, Tukey's test). There was no significant effect of the treatments on any of the PSII activity and performance parameters ($p > 0.05$, repeated measures ANOVA, Fig. 4).

Bacterial assemblage structure

After sequence processing, 3,799,629 and 1,951,629 partial 16S rRNA gene sequences could be assigned to the bacteria domain from Experiments 1 and 3, respectively. The total number of reads per sample ranged from 121,111 to 349,631 in Experiment 1 and from 56,424 to 206,922 in Experiment

3, and could be assigned to 862 and 815 ASVs in Experiment 1 and 3, respectively. Although treatment (including the initial samples) explained 26.6% of the variation in bacterial ASV composition in Experiment 1, as summarized by a Bray–Curtis dissimilarity matrix, the effect of treatment was not significant ($p = 0.155$, $F_{4,14} = 1.27$, PERMANOVA, Fig. 5a). In Experiment 3, however, the composition was significantly different between treatments ($p = 0.022$, $F_{4,12} = 2.9$, PERMANOVA, Fig. 5b) and explained 49% of the variation in the Bray–Curtis dissimilarity matrix. Pairwise comparison suggests that this difference was caused by the temporal change in assemblage composition from the initial to final sampling ($p < 0.05$, PERMANOVA), without any differences between pCO_2 levels ($p > 0.05$, PERMANOVA). This change is also reflected in alpha diversity, where the Chao1 index in Experiment 3 was significantly affected by treatment ($p < 0.001$, $F_{4,12} = 14.2$, ANOVA, Fig. 6b). The Chao1 index was reduced in all treatments during Experiment 3 ($p < 0.003$, Tukey's test), while no other diversity index was significantly affected by the treatments ($p > 0.05$, ANOVA, Fig. 6).

The bacterial assemblages in Experiment 1 and 3 were dominated by ASVs from the classes Bacteroidia, Alphaproteobacteria, and Gammaproteobacteria (Fig. 7a,b). Gammaproteobacteria were more prevalent in Experiment 3, where they contributed
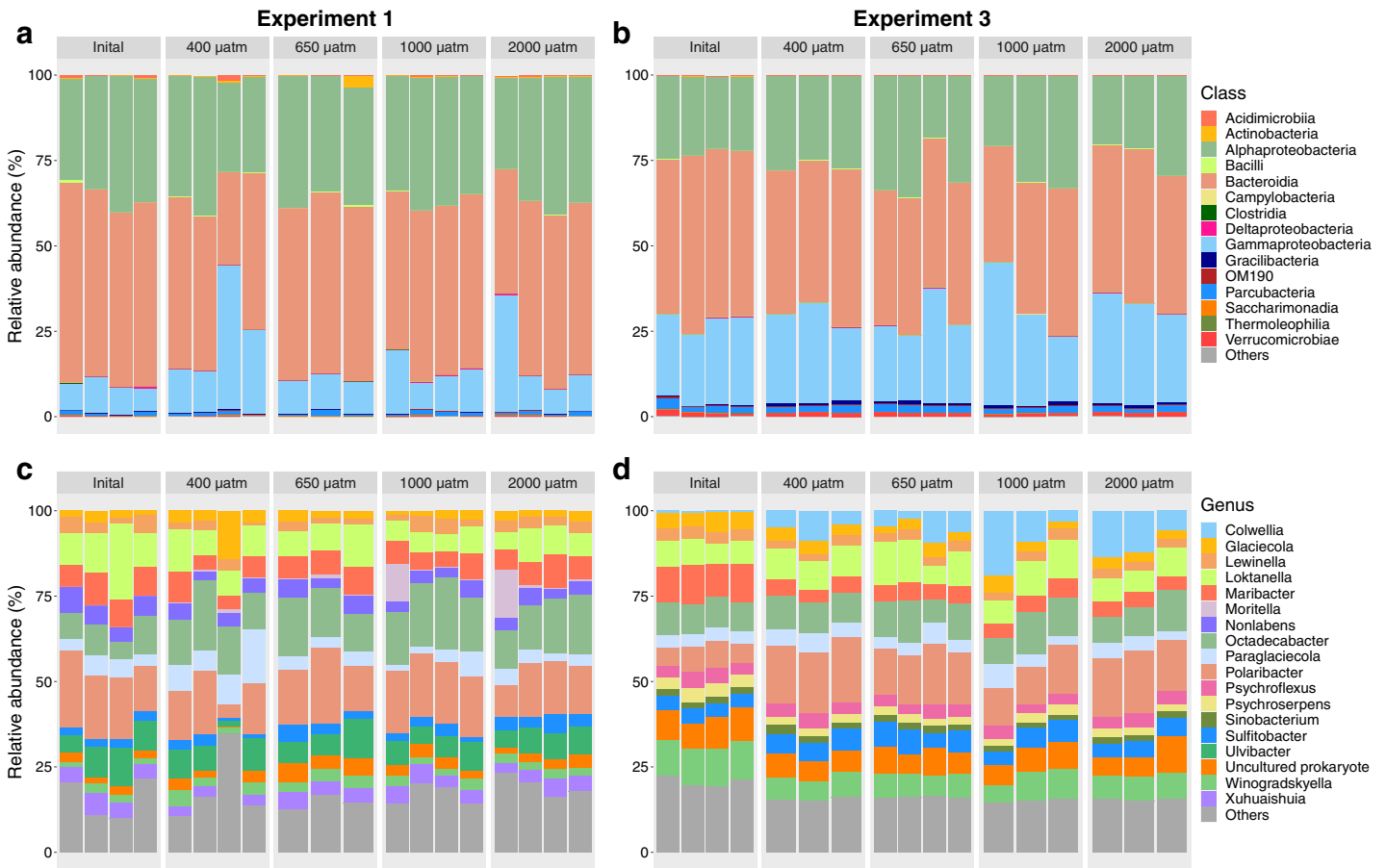
Fig. 7. Relative abundance of bacterial taxa in each sample, grouped by experimental treatment. The top 15 classes across all samples within Experiment 1 (**a**) and 3 (**b**) are color coded, where the lower abundance classes are grouped and shown in gray. The top 14 genera across all samples within Experiment 1 (**c**) and 3 (**d**) are color coded, where the lower abundance genera are grouped and shown in gray.

by 25.3% of the total abundance, compared to 14.1% in Experiment 1. Although the general assemblage structure remained unchanged during Experiment 1 (Fig. 5a), the abundance of *Octadecabacter* changed during the experiment ($p < 0.001$, $F_{4,14} = 5.6$, ANOVA, Fig. 7c). Here, members of *Octadecabacter* became more abundant in all pCO_2 treatments compared to the initial samples except for the 650 μatm treatment ($p < 0.05$ and $p = 0.07$, respectively, Tukey's test), although there were no significant differences between the pCO_2 treatments ($p > 0.7$, Tukey's test). The abundance of ASVs from the *Colwellia* genus increased significantly during Experiment 3 ($p < 0.001$, $F_{4,12} = 11.1$, ANOVA, Fig. 7d), where all treatments had higher abundances than the initial samples ($p < 0.001$, Tukey's test). However, there were no significant differences between pCO_2 treatments ($p > 0.13$, Tukey's test). The relative abundance of *Polaribacter* also changed during Experiment 3 ($p < 0.0001$, $F_{4,12} = 29$, ANOVA, Fig. 7d), where all treatments had higher abundances than the initial samples ($p < 0.01$, Tukey's test). Here, the abundance of *Polaribacter* in the 1000 μatm pCO_2 treatment was also lower compared to the 400 and 2000 μatm treatments ($p = 0.007$ and 0.026, respectively, Tukey's test).

An ANCOM procedure identified only a single bacterial ASV from Experiment 3 as differing significantly between the pCO_2 treatments (representing 0.11% of total abundance, $W_{0.7} = 470$, ANCOM). BLAST analysis of this sequence against the NCBI 16S rRNA gene database showed a 98.8% similarity to *Colwellia rossensis* strain S51-W. The relative abundance of this ASV was affected significantly by treatment ($p < 0.01$, $F_{4,12} = 5.9$, ANOVA). This ASV was absent in the initial samples, but appeared in higher abundance in the 2000 μatm treatment (0.3% $\pm$ 0.12% of total abundance) treatment compared to the 650 μatm (0.05% $\pm$ 0.04% of total abundance) treatment ($p < 0.05$, Tukey's test). No ASVs were identified as significant in the ANCOM procedure for Experiment 1.

Discussion

The vast majority of ocean acidification studies on sea-ice microbes have focused on single organisms from Antarctica (reviewed in McMinn 2017) or the Arctic (Torstensson et al. 2019; Kvernvik et al. 2020), although microbial

communities in Southern Ocean brine and bottom ice have recently been investigated (McMinn et al. 2017; Castrisios et al. 2018; Cummings et al. 2019). Our study is the first to report findings on sea-ice microbial community responses to ocean acidification in the Arctic Ocean and to consider different nutrient regimes. We observed no detectable change in the bottom-ice communities we examined in terms of biomass (as expressed by Chl *a* concentration and bacterial abundance), general bacterial assemblage structure, C/N ratio, photosynthetic activity, pEPS or DOC concentration after 10 d of pCO_2 treatment up to 2000 μatm (Table 3). Despite differences between Arctic and Antarctic sea ice and irrespective of the different inorganic nutrient levels and growth responses, the general lack of change in response to pCO_2 treatment in our experiments is similar to what has been observed in Antarctic sea-ice microbial communities, where no significant changes in photosynthetic activity or algal and bacterial growth were detected after incubations with pCO_2 up to 3700 μatm (McMinn et al. 2017; Cummings et al. 2019).

The core ecological processes of marine Arctic food webs appear resilient to climate change according to recent ecological modeling efforts (although these did not specifically consider sea-ice algae) (Griffith et al. 2019), and coastal Arctic phytoplankton from 20 to 50 m appear largely insensitive to ocean acidification (Hoppe et al. 2018a,b). The Arctic Ocean has a limited capacity to buffer against decreases in pH (Shadwick et al. 2013), and salts, microorganisms, and gases from the water are concentrated in the porous matrix of sea ice during the freezing process, creating enriched brines within the ice compared to surrounding waters. Brine trapped within the sea ice thus becomes oversaturated with CO_2 during ice formation. In spring, however, primary production increases in the ice and the carbonate system in the brine equilibrates with the surrounding water and air, causing CO_2 undersaturation, and potentially depletion, in the ice relative to the surrounding water (Geilfus et al. 2012). As a result, microorganisms in sea ice experience more extreme seasonal variation in pCO_2 (from 0 to 1800 μatm within a seasonal cycle; Geilfus et al. 2012) compared to most plankton in surface waters of the Arctic Ocean (normally ranging between 250 and 400 μatm; Yasunaka et al. 2016), suggesting that sea-ice microorganisms can tolerate large variations in pH, making them less susceptible to the 0.45 decrease predicted for the surface Arctic Ocean by 2100 (Steinacher et al. 2009). Not surprisingly, most ocean acidification studies on sea-ice algae using concentrations of pCO_2 to 3700 μatm have reported no effect, or small positive or negative effect sizes, relative to other environmental factors related to climate change (Torstensson et al. 2012; McMinn et al. 2017; Cummings et al. 2019; Torstensson et al. 2019). However, the growth of Antarctic sea-ice algal communities appears to be moderately affected by changes in the carbonate system as pCO_2 levels reach more extreme (up to 6000 μatm) values (McMinn et al. 2014), suggesting that the tipping point for these

communities is likely much higher than the changes in atmospheric pCO_2 that are expected within the century. The pCO_2 of Arctic sea ice may reach more extreme values (e.g., up to 1800 μatm pCO_2 in early spring) during sea-ice growth (Geilfus et al. 2012), but extreme values are unlikely for the bottom-ice community during summer, as in our study.

We tested whether increased CO_2 availability may cause carbon overconsumption (Toggweiler 1993) in sea-ice algal communities and thus stimulate excretion of organic carbon from the cells, as observed in phytoplankton from Kongsfjorden, Svalbard (Engel et al. 2013), and in the sea-ice alga *N. lecointei* under nutrient-replete conditions (Torstensson et al. 2015b). Although slight positive trends were observed in sea-ice sections incubated under nutrient-replete conditions (Experiments 1 and 2; Fig. 3), no significant increases in bacterial abundance, DOC or pEPS concentrations were detected in any of the experiments, suggesting that overproduction of extracellular organic carbon in response to higher pCO_2 was negligible in the time frame of our experiment. We observed a significant decrease in pEPS concentration under 650 μatm pCO_2 in Experiment 3, but whether that response represents a true treatment effect would require further investigation as it was inconsistent with responses in flanking treatments. DOC clearance, however, can be rapid in Arctic waters, with significant amounts of sea-ice-derived DOC utilized within days by Arctic bacterioplankton (Niemi et al. 2014). As no significant changes in bacterial abundances between the pCO_2 treatments were detected in our study, we believe that a masking of potential differences in DOC excretion by increased DOC uptake was unlikely.

In the central Arctic Ocean, sea-ice algae have been reported to excrete large amounts of DOC, possibly stimulated by the onset of nutrient deficiency in summer (Gosselin et al. 1997). By end of summer, as in our study, nutrient-stressed sea-ice algae in the oligotrophic Arctic were already experiencing low inorganic nitrate levels, and therefore may have been less likely to be affected by additional DIC (i.e., initially had a high inorganic C/N ratio). In our experiments, pEPS concentrations followed a different temporal pattern than algal and bacterial growth, with pEPS concentrations decreasing during Experiment 1, and increasing in Experiments 2–4 (Table 3), with the increase probably linked to the nitrate depletion that was apparent by the end of Experiments 2–4. Lower initial inorganic nutrient concentrations in Experiment 4 also resulted in increased organic C/N ratios (Table 3), yet did not stimulate a measurable effect of pEPS accumulation in response to elevated pCO_2 in 10 d, demonstrating that ocean acidification did not promote carbon overconsumption.

Future changes in ocean pCO_2 in the central Arctic Ocean will likely be accompanied by lowered nutrient concentration due to reduced upward ocean mixing (Randelhoff and Guthrie 2016). We investigated the role of inorganic nutrient concentration on the microbial response to ocean acidification by

incubating sea ice in seawater from two different water masses, which resulted in different growth responses of both ice algae and bacteria. For instance, no accumulation of Chl *a* was observed during Experiment 4, whereas it increased slightly during Experiment 1 and substantially during Experiments 2 and 3. The differences in growth resulted in a wide range of organic C/N ratios (from 7.7 to 18.3), enabling us to test the hypothesis that CO_2 affects sea-ice microbial communities under different nutrient conditions. Although our experiments were performed under different nutrient regimes, and the microbial communities developed differently during the different experiments, the pattern was generally not affected by pCO_2 treatment. Microorganisms adapted to the variable conditions of sea ice are therefore more likely to be tolerant of changes in carbonate chemistry than coastal phytoplankton assemblages (Hoppe et al. 2018*b*).

The photophysiology of Antarctic sea-ice algal communities appears to be somewhat reduced by high reductions of seawater pH (from 7.66 to 6.39, ΔpH = −1.27) when melted out of the ice (Castrisios et al. 2018). The photophysiology of the ice-algal aggregates in our Experiment 3, however, was not affected by the reduced pH (Fig. 4; Table S3), possibly due to the more modest pH shift (from 8.07 to 7.42, ΔpH = −0.65) compared to the latter study. Other studies on natural sea-ice algal communities have observed no change in F_v/F_m from pH 8.66 to 7.19 (ΔpH = −1.47; McMinn et al. 2014). Yet, negative responses to ocean acidification have recently been reported for both F_v/F_m and $rETR_{max}$ in sea-ice diatom cultures, probably due to changes in ion homeostasis or due to oxidative stress (Torstensson et al. 2019; Kvernvik et al. 2020). The diversity of natural sea-ice algal communities may buffer against this stress, as the PSII of sea-ice algal communities appears to be quite robust to pH changes expected in Arctic surface waters within this century (ΔpH = −0.45). Both F_v/F_m and $rETR_{max}$, however, can remain unchanged in sea-ice algae, even when growth rate has changed in in response to increased pCO_2, further suggesting that these measurements may not be sensitive enough to detect the stress responses expected from ocean acidification in diverse sea-ice algal communities (McMinn et al. 2017). Elevated pCO_2 may therefore be more likely to cause measurable effects in carbon assimilation than PSII performance by natural communities.

The effectiveness of carbon-concentrating mechanisms is believed to play an important role in the prediction of changes in microalgal composition as a response to human activities that affect inorganic nutrient stoichiometry, such as ocean acidification (Raven et al. 2011). However, most psychrophilic diatoms are known to maintain effective carbon-concentrating mechanisms and produce high concentrations of Rubisco (Tortell et al. 2013; Trimborn et al. 2013; Young et al. 2015a). At the same time, investments in carbon-concentrating mechanisms are likely less costly for psychrophiles due to the high solubility of CO_2 in cold water (Young et al. 2015*b*). Growth of the Antarctic sea-ice diatom

Nitzschia lecointei was only positively affected by increased pCO_2 when combined with elevated temperature (Torstensson et al. 2013), further supporting that sea-ice diatom growth is not limited by CO_2 at low temperature. As a result, elevated CO_2 levels may have less impact on primary production in psychrophilic microalgae compared to their temperate counterparts and may explain why the growth of sea-ice algal communities appeared insensitive to ocean acidification in our study.

The bacterial assemblages in the two experiments examined (Experiments 1 and 3) were dominated by psychrophilic and psychrotolerant taxa commonly found in Arctic sea ice, such as the genera *Polaribacter* (Bacteroidia), *Octadecabacter* (Alphaproteobacteria), and *Colwellia* (Gammaproteobacteria) (Boetius et al. 2015), though the communities developed differently during the two experiments (Fig. 7). The decrease in Chao1 richness during Experiment 3 (Fig. 6b) may have been in response to the algal growth that occurred, which would have provided DOC and EPS for opportunistic bacterial taxa to outcompete rare taxa. Gammaproteobacteria were generally more abundant in Experiment 3 than in Experiment 1, possibly owing to their abilities to exploit various organic compounds excreted by *M. arctica* (Fernández-Méndez et al. 2014; Rapp et al. 2018). During Experiment 3, ASVs from the genus *Colwellia*, known for its genetic capacity to degrade a wide range of released organic compounds (Methé et al. 2005), became noticeably more abundant in all treatments. ASVs from the genus *Polaribacter* also became more abundant, though less so in the 1000 μatm pCO_2 treatment compared to 400 and 2000 μatm pCO_2 treatments. Because false discovery rates can be high when comparing relative abundances directly (Mandal et al. 2015), an ANCOM approach was also used. This analysis detected only a single ASV (of the 815 ASVs), from the *Colwellia* genus, that differed between the pCO_2 treatments, indicating that the short-term effect of ocean acidification on Arctic sea-ice bacterial community composition is minor or negligible.

During Experiment 1, the overall bacterial assemblage structure remained unchanged (Fig. 7a,c). Here, the abundance of *Colwellia* remained low throughout the experiment, which may be explained by the slow algal growth and therefore, low rates of algal DOM excretion. These results for sea-ice bacterial communities in the central Arctic Ocean are thus similar to those of a previous study of coastal Arctic bacterioplankton, which showed negligible effects of ocean acidification on bacterial assemblage structure (Roy et al. 2013). Complex interactions within natural bacterial populations may make bacterial assemblages more resistant to ocean acidification, as suggested by Wang et al. (2015), but sea-ice bacteria may be insensitive to the pH reductions applied in our study because the sea-ice environment naturally confronts them with large variations in pH and pCO_2. The unchanged bacterial community structure we observed in Experiment 1 probably also reflects unchanged labile DOM abundance

and composition, given that the bulk algal community was unaffected by elevated pCO_2.

The limited duration of our experiments constrains how the results may be interpreted and extrapolated, as some effects of increased pCO_2 may not be detected in sea-ice algae—particularly some diatoms—until after several months of treatment (Torstensson et al. 2015*b*). The duration of our experiments was kept short to keep the ice-core sections intact throughout the experiments and to reduce bottle effects and artifacts from nutrient exhaustion. Even at $-1.7°C$, some ice melting could be detected after 10 d from the decrease in salinity over time relative to the more saline water from 1000 m. Nevertheless, intact algal filaments were visually detected inside the ice at 10 d, confirming the Chl *a* data that showed these ice-adapted algae had continued to grow within their sampled habitat, despite perturbation.

The measured pCO_2 levels in our incubations largely fell below the targeted values of 400, 650, 1000, and 2000 μatm (Tables 2, S1–S4), so that at time points where CO_2 had been reduced significantly, the carbonate system was readjusted toward target levels. Remeasuring levels after the CO_2 additions was not possible logistically, nor is determining exact pCO_2 levels in micrometer-scale brine pockets within sea ice yet feasible. Nevertheless, the average pCO_2 that the microorganisms experienced throughout the experiments was likely closer to the targeted values than indicated by the measured values, an aspect of our experiments to consider when comparing to other studies. With the drawdown and then addition of CO_2, the organisms in our study experienced variable pCO_2 levels, which may be regarded as more ecologically relevant for sea-ice microbial communities than a fixed level. Drawdown and replenishment occur in situ in sea ice due to primary production (Gleitz et al. 1995) and microbial respiration (Nguyen and Maranger 2011), as well as to temperature-driven precipitation and dissolution of ikaite crystals within Arctic sea ice (beyond the scope of this study, but see Rysgaard et al. 2011). Even CO_2 undersaturation, relative to seawater, is a realistic scenario for sea ice harboring high algal biomass (Geilfus et al. 2012; Tortell et al. 2013).

A major challenge with studying sea-ice microbial community responses to ocean acidification in shipboard experiments is the patchiness of sampling plots and limitations on replication, as also encountered during experiments conducted in situ (Cummings et al. 2019). To minimize spatial variability, we sampled duplicate ice-core sections for each experimental unit (and replicated time points in quadruplicate), from a floe with apparently homogeneously ice thickness in a relatively small area. Some degree of patchiness was still evident, given the observed within-group variability in the experiments involving intact ice sections (Experiments 1, 2, and 4). In Experiment 3, the algal aggregate community was homogenized before distribution into the experimental units, which resulted in lower within-group variability and greater statistical power. As the overall conclusion—that sea-ice

microorganisms are insensitive to ocean acidification—remained unchanged with the reduced heterogeneity in Experiment 3, we doubt that any potential treatment effects were masked by sample heterogeneity and limited statistical power in Experiments 1, 2, and 4.

Ocean acidification is occurring simultaneously with other changing environmental factors, including temperature, irradiance and nutrient levels, and we know from other studies that effects of ocean acidification on primary producers can be modulated in combination with these stressors (e.g., Torstensson et al. 2013; Hoppe et al. 2015). For instance, increased irradiance has been well-studied in combination with ocean acidification to simulate light conditions that algal cells will experience in a more stratified ocean, and the combination of high PAR and increased pCO_2 appears to have synergistic impacts on growth and photosynthesis in both temperate and Antarctic phytoplankton species (Gao et al. 2012; Hoogstraten et al. 2012; Trimborn et al. 2017). The primary productivity of the Southern Ocean phytoplankton species *Chaetoceros debilis* was reduced by elevated pCO_2 only when the cells were grown under dynamic light conditions, remaining unchanged under static irradiance (Hoppe et al. 2015). Given that sea-ice algae are currently low-light-adapted and will likely experience higher irradiances as a result of reduced ice thickness and the increasing occurrence of melt ponds (Arrigo et al. 2012), irradiance may be an important co-factor to consider in future studies of ocean acidification research on sea-ice algae. The central Arctic sea-ice algae of our study, however, along with their associated bacterial assemblages, appeared largely insensitive even to extreme ocean acidification (up to 2000 μatm pCO_2), highlighting the ecological importance and resilience of these sea-ice microorganisms even as pCO_2 continues to increase. We did not find any evidence of increased excretion of organic carbon (pEPS or DOC) from sea-ice algae as a response to elevated inorganic C/N ratios, irrespective of nitrate concentration. It seems that the greater threat to Arctic sea-ice microbial communities may be habitat loss caused by the continued reduction of sea-ice thickness and extent, which affects light penetration through the thinning sea ice (Arrigo et al. 2012) and can create a mismatch between the ice algal bloom and zooplankton grazing that, in turn, will have significant impacts on the whole Arctic ecosystem (Post et al. 2013).

References

Aitchison, J. 1982. The statistical analysis of compositional data. J. Roy. Stat. Soc. Ser. B. (Stat. Method.) **44**: 139–160.

Andrews, S. 2010. FASTQC. A quality control tool for high throughput sequence data. Available from http://www.bioinformatics.babraham.ac.uk/projects/fastqc/

Arrigo, K. R. 2017. Sea ice as a habitat for primary producers, p. 352–370. *In* D. N. Thomas [ed.], Sea ice. John Wiley & Sons, Ltd.

Arrigo, K. R., and D. N. Thomas. 2004. Large scale importance of sea ice biology in the Southern Ocean. Antarct. Sci. **16**: 471–486.

Arrigo, K. R., and others. 2012. Massive phytoplankton blooms under Arctic sea ice. Science **336**: 1408.

Bluhm, B. A., K. M. Swadling, and R. Gradinger. 2017, p. 394–414.*In* D. N. Thomas [ed.], Sea ice as a habitat for macrograzers. Sea ice: John Wiley & Sons, Ltd.

Boetius, A., and others. 2013. Export of algal biomass from the melting Arctic sea ice. Science **339**: 1430–1432.

Boetius, A., A. M. Anesio, J. W. Deming, J. A. Mikucki, and J. Z. Rapp. 2015. Microbial ecology of the cryosphere: Sea ice and glacial habitats. Nat. Rev. Microbiol. **13**: 677–690.

Bolyen, E., and others. 2019. Reproducible, interactive, scalable and extensible microbiome data science using QIIME 2. Nat. Biotechnol **37**: 852–857.

Bowman, J. S., S. Rasmussen, N. Blom, J. W. Deming, S. Rysgaard, and T. Sicheritz-Ponten. 2012. Microbial community structure of Arctic multiyear sea ice and surface seawater by 454 sequencing of the 16S RNA gene. ISME J. **6**: 11–20.

Boyd, P. W., and D. A. Hutchins. 2012. Understanding the responses of ocean biota to a complex matrix of cumulative anthropogenic change. Mar. Ecol. Prog. Ser. **470**: 125–135.

Caldeira, K., and M. E. Wickett. 2003. Oceanography: Anthropogenic carbon and ocean pH. Nature **425**: 365.

Callahan, B. J., P. J. McMurdie, and S. P. Holmes. 2017. Exact sequence variants should replace operational taxonomic units in marker-gene data analysis. ISME J. **11**: 2639–2643.

Castrisios, K., A. Martin, M. N. Müller, F. Kennedy, A. McMinn, and K. G. Ryan. 2018. Response of Antarctic sea-ice algae to an experimental decrease in pH: A preliminary analysis from chlorophyll fluorescence imaging of melting ice. Polar Res. **37**: 1438696.

Chierici, M., and A. Fransson. 2009. Calcium carbonate saturation in the surface water of the Arctic Ocean: Undersaturation in freshwater influenced shelves. Biogeosciences **6**: 2421–2431.

Cummings, V. J., N. G. Barr, R. G. Budd, P. M. Marriott, K. A. Safi, and A. M. Lohrer. 2019. *In situ* response of Antarctic under-ice primary producers to experimentally altered pH. Sci. Rep. **9**: 6069.

DelValls, T. A., and A. G. Dickson. 1998. The pH of buffers based on 2-amino-2-hydroxymethyl-1,3-propanediol ('tris') in synthetic sea water. Deep Sea Res. Pt. I **45**: 1541–1554.

Deming, J. W., and J. N. Young. 2017. The role of exopolysaccharides in microbial adaptation to cold habitats, p. 259–284.*In* R. Margesin [ed.], Psychrophiles: From biodiversity to biotechnology. Springer International Publishing.

DuBois, M., K. A. Gilles, J. K. Hamilton, P. A. Rebers, and F. Smith. 1956. Colorimetric method for determination of sugars and related substances. Anal. Chem. **28**: 350–356.

Engel, A., C. Borchard, J. Piontek, K. Schulz, U. Riebesell, and R. Bellerby. 2013. CO_2 increases ^{14}C-primary production in an Arctic plankton community. Biogeosciences **10**: 1291–1308.

Fernández-Méndez, M., F. Wenzhöfer, I. Peeken, H. L. Sørensen, R. N. Glud, and A. Boetius. 2014. Composition, buoyancy regulation and fate of ice algal aggregates in the Central Arctic Ocean. PLoS One **9**: e107452.

Fransson, A., and others. 2013. Impact of sea-ice processes on the carbonate system and ocean acidification at the ice-water interface of the Amundsen Gulf, Arctic Ocean. J. Geophys. Res. Oceans **118**: 7001–7023.

Gao, K., and others. 2012. Rising CO_2 and increased light exposure synergistically reduce marine primary productivity. Nat. Clim. Change **2**: 519–523.

Gardner, W. D., M. J. Richardson, and W. O. Smith Jr. 2000. Seasonal patterns of water column particulate organic carbon and fluxes in the Ross Sea. Antarct. Deep Sea Res. Pt. II **47**: 3423–3449.

Gattuso, J.-P., J.-M. Epitalon, and H. Lavigne. 2018. seacarb: Seawater Carbonate Chemistry. R package version 3.2.8. Available from http://CRAN.R-project.org/package=seacarb

Geilfus, N. X., and others. 2012. Dynamics of pCO$_2$ and related air-ice CO_2 fluxes in the Arctic coastal zone (Amundsen Gulf, Beaufort Sea). J. Geophys. Res. Oceans **117**: C00G10.

Gleitz, M., M. Rutgers v.d. Loeff, D. N. Thomas, G. S. Dieckmann, and F. J. Millero. 1995. Comparison of summer and winter inorganic carbon, oxygen and nutrient concentrations in Antarctic Sea ice brine. Mar. Chem **51**: 81–91.

Gosselin, M., M. Levasseur, P. A. Wheeler, R. A. Horner, and B. C. Booth. 1997. New measurements of phytoplankton and ice algal production in the Arctic Ocean. Deep Sea Res. Pt. II **44**: 1623–1644.

Griffith, G. P., H. Hop, M. Vihtakari, A. Wold, K. Kalhagen, and G. W. Gabrielsen. 2019. Ecological resilience of Arctic marine food webs to climate change. Nat. Clim. Change **9**: 868–872.

Haas, C. 2017. Sea ice thickness distribution, p. 42–64.*In* D. N. Thomas [ed.], Sea ice. John Wiley & Sons, Ltd.

Hoegh-Guldberg, O., and J. F. Bruno. 2010. The impact of climate change on the world's marine ecosystems. Science **328**: 1523–1528.

Hoogstraten, A., K. R. Timmermans, and H. J. W. de Baar. 2012. Morphological and physiological effects in *Proboscia alata* (Bacillariophyceae) grown under different light and CO_2 conditions of the modern Southern Ocean. J. Phycol. **48**: 559–568.

Hoppe, C. J. M., C. S. Hassler, C. D. Payne, P. D. Tortell, B. Rost, and S. Trimborn. 2013. Iron limitation modulates Ocean acidification effects on southern ocean phytoplankton communities. PLoS One **8**: e79890.

Hoppe, C. J. M., L.-M. Holtz, S. Trimborn, and B. Rost. 2015. Ocean acidification decreases the light-use efficiency in an Antarctic diatom under dynamic but not constant light. New Phytol. **207**: 159–171.

Hoppe, C. J. M., et al. 2018*a*. Resistance of Arctic phytoplankton to ocean acidification and enhanced irradiance. Polar Biol **41**: 399–413.

Hoppe, C. J. M., K. K. E. Wolf, N. Schuback, P. D. Tortell, and B. Rost. 2018*b*. Compensation of ocean acidification effects in Arctic phytoplankton assemblages. Nat. Clim. Change **8**: 529–533.

Horner, R., and others. 1992. Ecology of sea ice biota. Polar Biol. **12**: 417–427.

IPCC. 2013. Climate change 2013: The physical science basis. Contribution of working group I to the fifth assessment report of the Intergovernmental Panel on Climate Change. *In* T. F. Stocker and others. [eds.]. Cambridge University Press.

Krembs, C., H. Eicken, and J. W. Deming. 2011. Exopolymer alteration of physical properties of sea ice and implications for ice habitability and biogeochemistry in a warmer Arctic. Proc. Natl. Acad. Sci. **108**: 3653–3658.

Kvernvik, A. C., and others. 2020. Higher sensitivity towards light stress and ocean acidification in an Arctic sea-ice-associated diatom compared to a pelagic diatom. New Phytol. **226**: 1708–1724.

Lizotte, M. P. 2001. The contributions of sea ice algae to Antarctic marine primary production. Am. Zool. **41**: 57–73.

Mandal, S., W. Van Treuren, R. A. White, M. Eggesbø, R. Knight, and S. D. Peddada. 2015. Analysis of composition of microbiomes: A novel method for studying microbial composition. Microb. Ecol. Health Dis. **26**: 27663–27663.

Marschall, H.-P. 1988. The overwintering strategy of Antarctic krill under the pack-ice of the Weddell Sea. Polar Biol. **9**: 129–135.

Martin, M. 2011. Cutadapt removes adapter sequences from high-throughput sequencing reads. EMBnet J. **17**: 10–12.

McMinn, A. 2017. Reviews and syntheses: Ice acidification, the effects of ocean acidification on sea ice microbial communities. Biogeosciences **14**: 3927–3935.

McMinn, A., M. N. Müller, A. Martin, and K. G. Ryan. 2014. The response of Antarctic Sea ice algae to changes in pH and CO_2. PLoS One **9**: e86984.

McMinn, A., and others. 2017. Effects of CO_2 concentration on a late summer surface sea ice community. Mar. Biol. **164**: 87.

McMurdie, P. J., and S. Holmes. 2013. phyloseq: An R package for reproducible interactive analysis and graphics of microbiome census data. PLoS One **8**: e61217.

Meier, W. N., F. Fetterer, M. Savoie, S. Mallory, R. Duerr, and J. Stroeve. 2017. NOAA/NSIDC climate data record of passive microwave sea ice concentration, version 3. Data set ID G02202. NSIDC, National Snow and Ice Data Center. doi: 10.7265/N59P2ZTG

Methé, B. A., and others. 2005. The psychrophilic lifestyle as revealed by the genome sequence of *Colwellia psychrerythraea* 34H through genomic and proteomic analyses. Proc. Natl. Acad. Sci. USA **102**: 10913–10918.

Nguyen, D., and R. Maranger. 2011. Respiration and bacterial carbon dynamics in Arctic sea ice. Polar Biol. **34**: 1843–1855.

Niemi, A., G. Meisterhans, and C. Michel. 2014. Response of under-ice prokaryotes to experimental sea-ice DOM enrichment. Aquat. Microb. Ecol. **73**: 17–28.

Oksanen, J. and others. 2019. vegan: Community ecology package. R package version 2.5-6. Available from https://CRAN.R-project.org/package=vegan

Orellana, M. V., P. A. Matrai, C. Leck, C. D. Rauschenberg, A. M. Lee, and E. Coz. 2011. Marine microgels as a source of cloud condensation nuclei in the high Arctic. Proc. Natl. Acad. Sci. **108**: 13612–13617.

Orr, J. C., and others. 2005. Anthropogenic ocean acidification over the twenty-first century and its impact on calcifying organisms. Nature **437**: 681–686.

Pawlowicz, R. 2019. M_Map: A mapping package for MATLAB. Version 1.4k. Available from www.eoas.ubc.ca/~rich/map.html

Peng, G., W. N. Meier, D. J. Scott, and M. H. Savoie. 2013. A long-term and reproducible passive microwave sea ice concentration data record for climate studies and monitoring. Earth Syst. Sci. Data **5**: 311–318.

Platt, T., C. L. Gallegos, and W. G. Harrison. 1980. Photoinhibition of photosynthesis in natural assemblages of marine phytoplankton. J. Mar. Res. **38**: 687–701.

Post, E., and others. 2013. Ecological consequences of sea-ice decline. Science **341**: 519–524.

Quast, C., and others. 2013. The SILVA ribosomal RNA gene database project: Improved data processing and web-based tools. Nucleic Acids Res **41**: D590–D596.

R Core Team. 2018. R: A language and environment for statistical computing. Version 3.5.1. Available from https://www.R-project.org/

Randelhoff, A., and J. D. Guthrie. 2016. Regional patterns in current and future export production in the Central Arctic Ocean quantified from nitrate fluxes. Geophys. Res. Lett. **43**: 8600–8608.

Rapp, J. Z., M. Fernández-Méndez, C. Bienhold, and A. Boetius. 2018. Effects of ice-algal aggregate export on the connectivity of bacterial communities in the Central Arctic Ocean. Front. Microbiol. **9**: 1035–1035.

Raven, J. A., M. Giordano, J. Beardall, and S. C. Maberly. 2011. Algal and aquatic plant carbon concentrating mechanisms in relation to environmental change. Photosynth. Res. **109**: 281–296.

Roy, R. N., and others. 1993. The dissociation constants of carbonic acid in seawater at salinities 5 to 45 and temperatures 0 to 45 °C. Mar. Chem **44**: 249–267.

Roy, A. S., and others. 2013. Ocean acidification shows negligible impacts on high-latitude bacterial community structure in coastal pelagic mesocosms. Biogeosciences **10**: 555–566.

Rysgaard, S., and others. 2011. Sea ice contribution to the air–sea CO_2 exchange in the Arctic and Southern Oceans. Tellus B **63**: 823–830.

Sabine, C., and others. 2004. The oceanic sink for anthropogenic CO_2. Science **305**: 367–371.

Shadwick, E. H., T. W. Trull, H. Thomas, and J. A. E. Gibson. 2013. Vulnerability of polar oceans to anthropogenic acidification: Comparison of Arctic and Antarctic seasonal cycles. Sci. Rep. **3**: 2339.

Silsbe, G. M., and S. Y. Malkin. 2015. phytotools: Phytoplankton production tools. R package version 1.0. Available from https://CRAN.R-project.org/package=phytotools

Steinacher, M., F. Joos, T. L. Frölicher, G.-K. Plattner, and S. C. Doney. 2009. Imminent ocean acidification in the Arctic projected with the NCAR global coupled carbon cycle-climate model. Biogeosciences **6**: 1877–1882.

Straub, D., Blackwell, N., Langarica-Fuentes, A., Peltzer, A., Nahnsen, S., Kleindienst, S. 2020. Interpretations of Environmental microbial community studies are biased by the selected 16S rRNA (Gene) amplicon sequencing pipeline. Frontiers in Microbiology **11**: 550420. http://dx.doi.org/10.3389/fmicb.2020.550420

Toggweiler, J. R. 1993. Carbon overconsumption. Nature **363**: 210–211.

Torstensson, A., M. Chierici, and A. Wulff. 2012. The influence of increased temperature and carbon dioxide levels on the benthic/sea ice diatom *Navicula directa*. Polar Biol. **35**: 205–214.

Torstensson, A., M. Hedblom, J. Andersson, M. X. Andersson, and A. Wulff. 2013. Synergism between elevated pCO_2 and temperature on the Antarctic sea ice diatom *Nitzschia lecointei*. Biogeosciences **10**: 6391–6401.

Torstensson, A., J. Dinasquet, M. Chierici, A. Fransson, L. Riemann, and A. Wulff. 2015a. Physicochemical control of bacterial and protist community composition and diversity in Antarctic sea ice. Environ. Microbiol. **17**: 3868–3881.

Torstensson, A., M. Hedblom, M. Mattsdotter Björk, M. Chierici, and A. Wulff. 2015b. Long-term acclimation to elevated pCO_2 alters carbon metabolism and reduces growth in the Antarctic diatom *Nitzschia lecointei*. Proc. R. Soc. Biol. Sci. Ser. B **282**: 20151513. https://doi.org/10.1098/rspb.2015.1513

Torstensson, A., C. Jiménez, A. K. Nilsson, and A. Wulff. 2019. Elevated temperature and decreased salinity both affect the biochemical composition of the Antarctic Sea-ice diatom *Nitzschia lecointei*, but not increased pCO₂. Polar Biol. **42**: 2149–2164.

Tortell, P. D., and others. 2013. Inorganic C utilization and C isotope fractionation by pelagic and sea ice algal assemblages along the Antarctic continental shelf. Mar. Ecol. Prog. Ser **483**: 47–66.

Trimborn, S., T. Brenneis, E. Sweet, and B. Rost. 2013. Sensitivity of Antarctic phytoplankton species to ocean acidification: Growth, carbon acquisition, and species interaction. Limnol. Oceanogr. **58**: 997–1007.

Trimborn, S., S. Thoms, T. Brenneis, J. P. Heiden, S. Beszteri, and K. Bischof. 2017. Two Southern Ocean diatoms are more sensitive to ocean acidification and changes in irradiance than the prymnesiophyte *Phaeocystis antarctica*. Physiol. Plant. **160**: 155–170.

van Heuven, S., D. Pierrot, J. W. B. Rae, E. Lewis, and D. W. R. Wallace. 2011. MATLAB program developed for CO_2 system calculations. ORNL/CDIAC-105b. Carbon Dioxide Information Analysis Center, Oak Ridge National Laboratory, U.S. Department of Energy. doi:10.3334/CDIAC/otg.CO2SYS_MATLAB_v1.1

Vihma, T. 2014. Effects of Arctic sea ice decline on weather and climate: A review. Surv. Geophys. **35**: 1175–1214.

Wang, Y., and others. 2015. Bacterioplankton community resilience to ocean acidification: Evidence from microbial network analysis. ICES J. Mar. Sci **73**: 865–875.

Welschmeyer, N. A. 1994. Fluorometric analysis of chlorophyll *a* in the presence of chlorophyll *b* and pheopigments. Limnol. Oceanogr. **39**: 1985–1992.

Woosley, R. J., F. J. Millero, and T. Takahashi. 2017. Internal consistency of the inorganic carbon system in the Arctic Ocean. Limnol. Oceanogr. Methods **15**: 887–896.

Yasunaka, S., and others. 2016. Mapping of the air–sea CO2 flux in the Arctic Ocean and its adjacent seas: Basin-wide distribution and seasonal to interannual variability. Polar Sci **10**: 323–334.

Young, J. N., J. A. L. Goldman, S. A. Kranz, P. D. Tortell, and F. M. M. Morel. 2015a. Slow carboxylation of Rubisco constrains the rate of carbon fixation during Antarctic phytoplankton blooms. New Phytol. **205**: 172–181.

Young, J. N., S. A. Kranz, J. A. L. Goldman, P. D. Tortell, and F. M. M. Morel. 2015b. Antarctic phytoplankton downregulate their carbon-concentrating mechanisms under high CO_2 with no change in growth rates. Mar. Ecol. Prog. Ser. **532**: 13–28.

Conflict of interest
None declared.